Experimental Validation of an Optically Measured Digital Replica of a Geometrically Mistuned Rotor Using a System ID Approach

Alexander A. Kaszynski *

Universal Technology Corporation, Dayton, OH, 45434, USA

Joseph A. Beck † and Jeffrey M. Brown ‡

Air Force Research Laboratory, Wright-Patterson AFB, OH, 45433, USA

This work validates a digital replica of a mistuned rotor created from a point cloud produced from a structured light topological measurement system. The measurement system accurately captures the manufacturing deviations of each airfoil and allows prediction of the mistuned dynamic response of the rotor subject to harmonic excitation. A reverse engineering process is used to first create a nominal finite element model of the point cloud and subsequently transform each airfoil geometry to the measured point cloud. Model results are compared to a traveling wave excitation vibration test that approximates engine harmonic loading using phase shifted magnetic actuators. Uncertainties are assessed in point cloud collection, reverse engineering process, and the experiment. Results show minimal variation in the model predictions and experimental measurements. Comparison between analysis and test show excellent agreement, validating the process to create digital replicas that accurately predict complex dynamic behavior of rotor mistuned response.

Nomenclature

CMM	Coordinate Measuring Machine
CNC	Computer Numerical Control
CCD	Charge Coupled Device
DFT	Discrete Fourier Transform
EO	Engine Order
FEM	Finite Element Model
FMM ID	Fundamental Mistuning Model Identification
IBR	Integrally Bladed Rotor
ISA	Iterative Spring Analogy
NSMS	Non-Intrusive Stress Measurement System
RBF	Radial Basis Function
TSD	Tessellated Scan Data
TWE	Traveling Wave Excitation

*Research Engineer Contractor, Aerospace Systems Directorate, 1950 5th Street, Wright-Patterson AFB, OH, 45433, AIAA Member

†Aerospace Engineer, Materials and Manufacturing Directorate, Wright-Patterson AFB, OH, 45433, and Senior AIAA Member.

‡Senior Aerospace Engineer, Aerospace Systems Directorate, 1950 5th Street, Wright-Patterson AFB, OH, 45433, and Senior AIAA Member.

I. Introduction

Procedures to measure dimensions of manufactured components are an integral part of the production process for advanced components. The preponderance of measurement systems in practice are touch probe coordinate measurement machines (CMMs) capable of capturing precise coordinate locations with relative ease. Their data is used to ensure that manufactured parts are meeting their design intent within a given tolerance. While essential to the engineering process, these touch based systems are intended primarily for quality control and are limited in their ability to capture spatially dense data sets useful for creating precise digital replicas. While it is possible for the touch probe system to perform the task, procedurally it would require significant manual set up or CNC programming.[1] Instead, the metrology industry has been moving toward optical systems that use a structured light approach to measure the detailed topology of parts. The large measurement data sets, called point clouds, produced by these systems provide the opportunity to pursue creation of digital representations of the manufactured component in the form of CAD and finite element models (FEMs). This removes the conventional assumption that all manufactured parts respond as the FEM used in the design process had predicted and allows assessment of part-to-part variations in capability. This process is consistent with the Digital Twin philosophy that has been described by several authors.[2–4]

A challenging test case for the process of creating a component digital replica is the turbine engine integrally bladed rotor (IBR). An IBR is comprised of the rotating disk and airfoils of a conventional stage but is machined from a single metal forging. Its large and twisted airfoils can be closely spaced creating line of sight challenges for both laser and structured light measurement systems. The IBRs metallic surface also scatters projected light, leading to increased measurement noise or possibly no data collection at all. The sharp leading edges are similarly difficult to measure.[5] Beyond these geometry data collection difficulties, the physics of IBR structural dynamics are sufficiently sensitive to necessitate high accuracy in the digital reconstruction. All engine rotors are subject to structural mistuning, a characteristic defined by the blade-to-blade deviations in geometry and material properties that lead to variations in airfoil substructure resonant frequencies and mode shapes.[6] This breakdown in cyclic symmetry leads to system modes that couple and localize energy into a subset of the rotor airfoils, leading to forced response amplifications up to three times the design intent.[7] Since blade-to-blade mistuning is primarily caused by geometry variations on the order of several mils ($> \pm 0.004$"), leading to approximately $\pm$ 1% variations in airfoil substructure modal frequencies, it is clear that mistuned response is extremely sensitive to small deviations. Mistuning is frequently treated probabilistically to account for the chaotic nature of the phenomenon.[8,9] Given the challenge of collecting the geometry data, requirement for precise geometry measurement, and prediction of highly chaotic mistuned forced response, the IBR digital twin test case provides a rigorous assessment of the methods described in this work.

The following sections describe the procedures and results of the uncertainty quantification and validation. They begin with further description of the methodology employed to capture the IBR geometry using optical means, highlighting the accuracy and also the measurement challenges. Next, the process to convert the geometric point cloud into a FEM is discussed, highlighting its ability to produce a FEM optimally fit to the point cloud with consideration for mesh quality. The experimental setup is then reviewed, explaining the TWE system hardware and its own experimental calibration process to enforce consistent airfoil loading. With the experiment explained, a system identification process is described that allows extraction of airfoil subcomponent responses from the more chaotic response of the mistuned rotor system. These subcomponent responses allow for a rigorous validation of the predictions. And finally, the results of the comparison of the digital replica predictions to the experimental data are discussed.

A. Structured Light Topological Measurement

To measure parts, structured light measurement systems project sequences of parallel line fringe patterns. Three-dimensional images of these patterns are captured with high density charged coupled device (CCD) cameras that are similar to conventional digital cameras.[10] Image processing of the individual fringe distortion on the part generates point cloud coordinates. The capturing process is challenged by typical limitations of cameras including focal range and dynamic range. The focal range determines the distance the sensor head is offset from the measured part to capture a given volume of its geometry. Large focal ranges allow measurement of larger portions of parts, but point cloud measurements are more diffuse. Short ranges provide more point density, but for large part, numerous images would be needed and the method to compound

the set into a whole can introduce error. Focal range is a function of the fixed length of the CCD cameras and user experience is helpful in selecting appropriate value for a given component. The dynamic range of the sensor also determines the ability of the sensor to capture geometry coordinates. Existing systems use methods to extend the dynamic range of the CCDs by taking multiple images of a projected fringe pattern at various exposures and combining results. While effective, current systems are still challenged by reflective objects that angle fringe images away from the CCD sensors, or on the other end of the spectrum, reflecting towards the sensor and overexposing the image.[11] Reflectivity can be countered with light spray coating such as fluorescent penetrant inspection FPI developer or titanium dioxide. FPI developer is approximately 1 mil (0.001") while titanium dioxide can be as thin as 0.03 mil.[1]

The measurement process for a full IBR is approximately four hours and can be automated with relative ease as complicated CNC programming is not needed. Instead, a series of scanner head height and angle are needed with the measured part being rotated either manually or by computer controlled rotary tables. A four hour measurement generates a large number of image captures that are combined into a common reference frame using photogrammetry. Photogrammetry is the analysis of reference markers in photographic images to determine their location in space. Each photogrammetric measurement is taken at the same time as the structured light measurements and its results are used to align multiple scans into a common reference frame. Reference markers are required on the part if it needs to be moved from its initial reference frame. In other words, an IBR does not need to have reference stickers on its surface if it merely rotates on an automated table, but if it needs to be picked up and flipped to capture features on the other side, they would be. By using external reference markers and determining practical fixturing that allows full part measurement without its movement, measurements can be made without referencing the part. The optical scanner setup on a rotating table can be found in Figure 1.

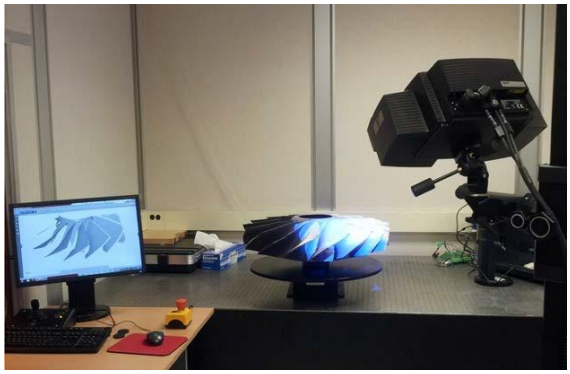

Figure 1: 3D Optical Scanner Setup

Published accuracy studies show an ability to measure components to within 0.0003".[1,12] This is significantly smaller than typical airfoil manufacturing deviations and helped motivate further investigation of building digital replicas of measured IBRs. The referenced work[12] also looked at the impact of scan-to-scan measurement variations and found, for the modes investigated, a small impact on the predicted response variation of reverse engineered digital replicas. This reverse engineering process is described in more detail in the following section.

B. Reverse Engineering Digital Replicas through Mesh Metamorphosis

While there are several methods of collecting point clouds of parts, there are few options available to readily create FEMs that conform to the data. Two approaches can be pursued to facilitate this process, first, creating CAD geometry entities that fit the point cloud data and then decomposing that geometry such that it can be modeled with a hexahedral element dominant mesh. Hex dominance is pursued for the mistuned IBR problem because of their convergence characteristics that lead to higher accuracy.[13] This CAD-based approach was pursued and automated for large rotor sets, but there were several limitations.[12] Foremost was the need for significant CAD and FEM specialist time to create parametric models with the required robustness to work for a large population of measured parts. Even when complete, the process made approximations in geometry particularly at the airfoil fillet and blade tip region which both exhibit complex curvatures not easily parameterized.

The alternative to the parametric CAD approach is to directly update the nodal locations of an existing nominal finite element model so that they conform to the point cloud measurements. Bypassing the CAD model construction and FEM meshing process leads to dramatic reduction in modeling resources and allows for mesh adaptations that are unconstrained by the definition of model design parameters. These benefits of a mesh updating approach are counterbalanced by the reality that the updating process requires solutions to its own set of implementation challenges. The updating process is largely driven by the relationship between surface normals of the FEM and the tessellated scan data (TSD) of the point cloud. Using these allows the

projection of nodes toward the TSD surface and finding the intersection. While straightforward in concept, this approach breaks down at areas of high curvature such as found at airfoil leading edges. The curvature leads to high sensitivity in the direction of projection and leads to cases where the projection completely misses the target surface. The projection also commonly fails at the intersection of two surfaces, such as where the airfoil intersects the disk rim. At these regions the node projections may move to the incorrect surface and lead to highly distorted elements. If the portions of the FEM are not contained within the boundaries of the point cloud, like at the airfoil tip of a overly twisted blade, the FEM updating will not be able to differentiation whether to project to pressure or suction side airfoil surfaces. Even when the exterior FEM nodes find their place on the point cloud surface, the state of the interior nodes must also be managed to ensure mesh quality is retained.

These challenges were addressed by Kaszynski et al. and the algorithm MORPH,[14] was applied to an academic rotor. The methodology has been applied to several other IBR and inserted airfoils and has proven to be robust. It utilizes a novel technique to generate an updated FEM through the use of an intelligent neural network model of the FEM and the TSD. MORPH requires an initial nominal model of reasonable accuracy to begin the mesh morphing process. For mistuned IBRs, this "seed" model is a nominal tuned approximation whose surface and interior nodes will be modified. This initial model can either be nominal FEM available from the design process or a model reverse engineered from optical scan data. MORPH applied to IBRs is both noise tolerant and capable of capturing all line of sight geometry on existing hardware. The algorithm follows:

1. Compute FEM surface node normal vectors and determine distance from nodes to TSD using algorithm presented in Moller et al.[15] Each FEM node normal N is defined by origin O, location of the node, and direction D representing the normal vector of that node as shown below in Equation 1

$$N(t) = O + tD \tag{1}$$

2. Calculate node displacement vectors using a neural network based alignment method with a scoring based on FEM node to TSD face distance and alignment. This score S is computed by Equation 2 where d_f is a vector of the distances between the FEM node and the center of adjacent TSD faces

$$S = \frac{d_{min}\frac{1}{d_f} + \hat{n}_f \otimes \hat{n}_n}{2} \tag{2}$$

3. Distribute local node displacements among adjacent nodes using a radial basis function (RBF), thereby allowing nodes to influence their neighbors through the Gaussian RBF φ. The node-to-node influence is dependent on the geodesic distance between two nodes through the 3D FEM and is given by Equation 3 where τ is the linear influence coefficient, ϵ is the exponential influence coefficient, and r is the geodesic distance through the 3D mesh.

$$\varphi(r) = \tau e^{-(\epsilon r)^2} \tag{3}$$

4. Sum the RBF displacement vectors for all nodes and update node positions. Limit maximum node movement by a fraction of the global average element edge length.

5. Check updated element shape. Limit node movements that would corrupt surface elements (e.g. aspect ratio and skew).

6. Iterate through steps 1-4 while modifying the RBF based on the rate of change of node positions. Run until FEM to TSD distance converges.

7. Place surface mid-side nodes of quadratic elements between edge nodes. Compute mid-side node normal vectors based on the average of the edge node vectors and move those nodes directly along the normal vectors to the surface of the TSD.

8. Propagate surface node movements internally using the iterative spring analogy (ISA).[16]

9. Optimize element quality using a variety of approaches, to include the geometric element transformation method.[17]

The MORPH process has been demonstrated to effectively update nominal FEM to point cloud data from a structured light system. This paper describes the comparison of the forced response predictions of the updated model with engine representative experimental results. The following comparison is validating the entire reverse engineering process for the digital replica and is an assessment of the accuracy of point cloud measurement, FEM updating, and the accuracy of the FE methods ability to predict the highly chaotic forced response behavior of mistuned IBRs. The description of the validation effort begins with explanation of the experimental equipment and procedures that mimic operating engine behavior.

C. Traveling Wave Excitation System

Turbine engines compress air in their fan and compressor stages using a combination of static stator airfoils and the rotating airfoils of IBRs. As the rotating airfoils pass the stators they cross through their lower pressure wakes, producing a sinusoidal or harmonic load as a function of time. Each airfoil experiences the same load magnitude though at offset phase angles that are a function of number of rotor airfoils and the engine order (EO) excitation. EO excitation refers to the number of upstream or downstream disturbance an IBR airfoil passes, such as the number of stator airfoils. Mistuned IBRs show varying response amplifications at each EO excitation and therefore it is a loading characteristic that must be included in bench testing.

To simulate EO loading outside an actual engine test, a traveling wave excitation (TWE) system is employed. The systems components are a IBR mounting fixture, electromagnetic actuators, a fixture for holding the actuators at fixed locations, a function generator, a phase shifting amplifier, impedance matching transformers, and a computer with control software as shown in Figure 2. For non-magnetic components, small metal plates are temporarily attached to the blade excitation location. The mass of the metal plate is very small compared to the airfoil mass and does not significantly impact response. Airfoil response is measured with a scanning laser vibrometer.

Airfoil loading is sensitive to the placement of the electromagnetic actuators and small deviations in the air gap between the two can lead to test inaccuracies. To account for this a calibration process is first conducted that ensures each airfoil receives equivalent loading. The process requires exciting a single blade and recording response at all other blades. This process is repeated for all blades. Results are used in a matrix solution that solves for calibration factors that ensure that each blade is loaded and within expected phase angle within a small tolerance. Details of this process can be found in research by Holland et al. in *Testing and Calibration Procedures for Mistuning Identification and Traveling Wave Excitation of Blisks*.[18]

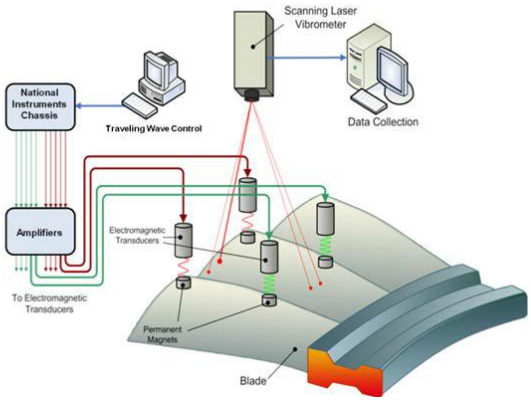

Figure 2: TWE Setup

Experimental results from the TWE capture the system response of the IBR as an assembly of airfoils and disk. For validation purposes, it is desirable to decompose this system response into the characteristics of each airfoil substructure. The following section describes the method applied to both the analytical an experimental results.

D. Mistuned System Identification Process

Tuned rotor and mistuned airfoil modal properties can be extracted from the IBR system response through system identification of the TWE forced response data. The parameters are determined using the fundamental mistuning model identification (FMM ID) approach of Feiner and Griffin.[19,20] While the basic form of FMM ID requires input of tuned system frequencies, the approach used here is their completely experimental method based solely on TWE measurements. Tuned and mistuned forced response results are predicted with the identified parameters and the FMM model.

FMM is an efficient approach to mistuning modeling that, through the assumption of an isolated mode family, reduces response prediction inputs to the tuned system frequencies and frequency deviation of each blade. The derived FMM equation is

$$\left(\Omega^{\circ 2} + 2\Omega^{\circ}\bar{\Omega}\Omega^{\circ}\right)\vec{\beta_j} = \omega_j^2\vec{\beta_j} \tag{4}$$

where Ω° is a diagonal matrix of the tuned system frequencies, $\bar{\Omega}$ is a matrix of the discrete Fourier transforms of the sector frequency deviations, β_j is the eigenvector of weighting factors used with the $\vec{\phi_j}$ tuned modes to reconstruct mistuned modes, and ω_j are the system eigenvalues. Solving the FMM inverse problem of known mistuned system modes and frequencies, the airfoil frequency deviations and tuned modes can be determined. The appropriately rearranged FMM equation for this process is

$$2\Omega^\circ\overline{\Omega}\left[\Omega^\circ\vec{\beta_j}\right] = \left(\omega_j^2\mathbf{I} - \Omega^{\circ 2}\right)\vec{\beta_j} \tag{5}$$

Further algebra to isolate measured TWE data on the right hand side leads to the form

$$\Omega^{\circ 2}\vec{\beta_j} + 2\Omega^\circ\Gamma_j\vec{\omega} = \omega_j^2\vec{\beta_j} \tag{6}$$

where $\vec{\omega}$ is the vector of DFT sector frequency deviations and Γ is a matrix whose elements are the product of Ω° and β_j. With the following alteration

$$\Omega^{\circ 2}\vec{\beta_j} = B_j\vec{\lambda^\circ} \tag{7}$$

$\vec{\lambda^\circ}$ becomes the vector of squared tuned frequencies and the B_j matrix combines the each j measured vectors β_j. Now that the rotor mistuning is a vector so it can be solved for with linear algebra as follows

$$\begin{bmatrix} B_j \\ 2\Omega^{\circ\Gamma_j} \end{bmatrix}\begin{bmatrix} \vec{\lambda} \\ \vec{\omega} \end{bmatrix} = \omega_j^2\vec{\beta_j} \tag{8}$$

In addition, by using response data from several system modes, errors from measurement variations are reduced. To incorporate additional modes into Equation 8, each is concatenated after the last row of the preceding measurement resulting in a stacked block of matrices.

A least squares approach of the inverse problem leads to the best fit solution to the multiple mistuned modes. These equations are then used with the addition of a constraint to resolve indeterminacy and then solved as a least squares solution

$$\begin{bmatrix} \vec{\lambda^\circ} \\ \vec{\omega} \end{bmatrix}_{(k)} = Lsq\left\{\begin{bmatrix} \tilde{B} & 2(\tilde{\Omega^\circ\Gamma})_{(k-1)} \\ 0 & \vec{c} \end{bmatrix}, \begin{bmatrix} \tilde{\vec{r}} \\ 0 \end{bmatrix}\right\} \tag{9}$$

where $\tilde{\vec{r}}$ is the multiple mode stacked block of the $\omega_j^2\vec{\beta_j}$ terms on the right side of Equation 8 and $\vec{c}$ is a row vector beginning with 1 and all other elements zero. The subscript k refers to the iteration number of the nonlinear solution and the tildes signify a matrix of stacked blocks of matrices of each mode retained in the solution.

For the purpose of validation, this process is applied to the experimental TWE data and the predicted system response from the digital replica. Comparisons will be made to identified blade sector frequency deviations, system tuned frequencies, and blade response amplification. Blade response amplifications are predicted using the identified frequency deviations, $\vec{\omega}$, and tuned system frequencies $\vec{\lambda^\circ}$ using Equation 4.

II. Analytical Model Validation

A production IBR was used to evaluate the effectiveness of the optically based geometric mistuned model (GMM). A non-academic rotor was chosen to provide evidence to support the digital twin concept and steps have been taken in this paper to obscure the identity of the IBR, but not the mistuned results thereof. The production IBR is a 22 bladed first stage compressor CNCed from a single forging of titanium to minimize material variation (elastic modulus, density) between blades. The FEM for the rotor was created from existing design CAD, and as this is a bending dominant structure, the FE mesh contains entirely quadratic hexahedral elements with mid-side nodes for more accurate element shape functions. The original tuned model was generated by replicating a cyclic sector about the central Z-axis to create a full 360° rotor containing 37,488 elements and 205,788 nodes. Figure 3 shows a fraction of the full IBR, though the figure has been distorted and skewed to eliminate traceability of the IBR.

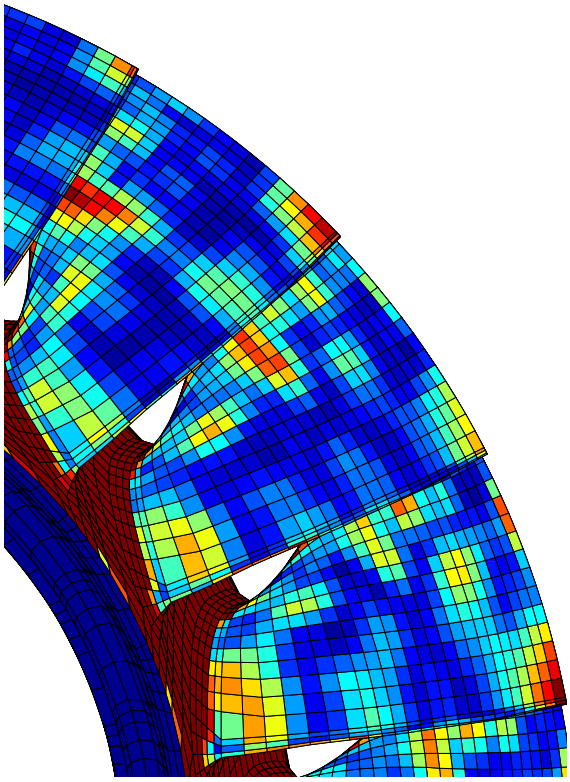

Figure 3: GMM to Tuned FEM Variation (0.001" - 0.06") (Model Distorted)

TSD was collected from a production rotor using with a 11.81 in × 11.81 in scan volume allowing for a minimum feature detection of 0.0005 in. The initial TSD contains 10^6 geometry points and 2×10^6 triangular faces. The collected point cloud was aligned to the FEM using an iterative closest point algorithm to translate and rotate the target point cloud to a reference point cloud (surface nodes of the FEM) by iteratively minimize the distances between the two. The rotor was aligned as to have the same blade ordering as in the experimental test given an index marker (weep hole) on the disk of the FEM.

Using the mesh metamorphosis algorithm previously described, the surface nodes of the FEM were modified to match the geometry of the TSD. The mean variation between the FEM surface nodes and TSD for a single rotor was approximately 7 mil (0.007"), while peaking to 60 mil (0.060") on certain portions of the IBR, specifically the blade root and blade tips. Figure 3 also shows the variation between the FEM and the TSD for rotor 1 with the blue portions indicating low variation and red indicating high variation. Even given the large deviation scale (0.001" to 0.06"), the as manufactured IBR shows significant variation from the design intention. Of particular interest is the fillet and platform, one of the most difficult areas for accurate CAD and FEM generation. The accuracy of the blade-disk interface is crucial to accurate calculation of system mode shapes since modal energy transfer between blades occurs in this interface.

A. Rotor 1 Analysis: Repeated Single EO at 1T

The experimental data was collected in several varied approaches in order to validate the FMM ID process and examine for potential variations in the TWE analysis. Understanding that experimental results have inherent uncertainty, experimental data for the IBR was collected 15 times for the 1^{st} torsional mode at EO 4. The first torsional mode (1T) was selected in order to maximize the signal to noise ratio since the blade would be excited on the tip of the trailing blade edge and measured at the tip of the leading blade edge, and ideal setup for the 1T mode. The repeated data was collected by rotating the rotor on the test stand to test for variation in calibration accuracy, and the tests were repeated five times per rotation to test for measurement noise from the laser vibrometer. The frequency response function (FRF) for a single blade for all results is shown in Figure 4. The actual amplitude of the response has been normalized as it is the mode shape, not the magnitude of the response, that is the goal of the experimental data collection. As such, the maximum amplitude of the response for the frequency range 3850 - 3910 Hz has been normalized to 1 for the peak response. However, despite this, there appears to be variation between the runs in both frequency and mode shape for the single blade response despite recalibration. As it will be shown, these small variations

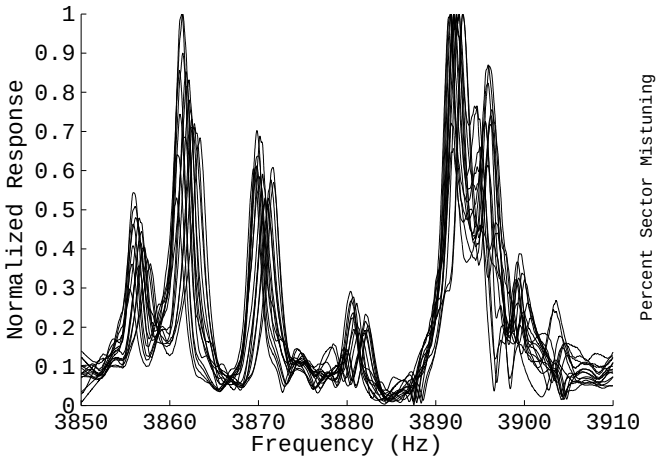

Figure 4: Variation in Experimental FRF

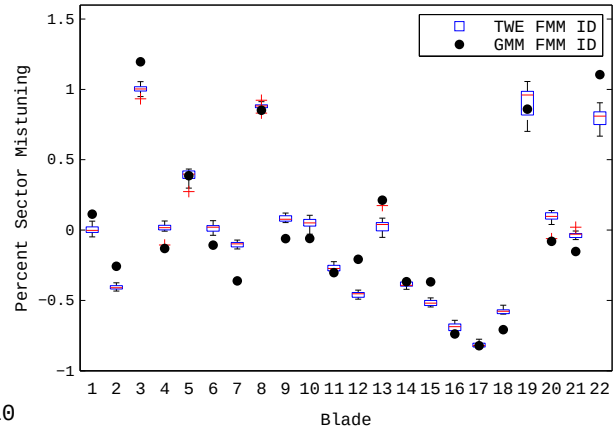

Figure 5: Sector Mistuning Variation

will are significant when applying FMM ID.

The extraction of mode shapes for FMM ID is a two step process. First, the results from all 22 blades are averaged into a single FRF and the system mistuned modes are selected by identifying the peaks responses of the combined data. These are the frequencies of the mistuned system, eigenvalues ω_j. The relative position of each blade is then recorded for each system mode and normalized to produce a matrix of system mode shapes. The goal of this analysis is to compute the blade response amplification relative to the ideal, tuned rotor. As such, FMM ID is used to determine the tuned system and mistuned system response given the mistuned mode shapes for a single system mode (e.g. 1T). The tuned modes are solved for using a least squares approximation according to Equation 8, as with the mistuned sector variation β_j. The sector mistuning variation $\vec{\omega}$ for the IBR is shown in Figure 5, and this plot shows a small variation between the repeated experimental data and a strong correlation ($R^2 = 0.923$) between the mean experimental results and the analytical results. The agreement indicates that the geometric variation, as captured by the relative nodal displacements between blades, is the main driver in blade-to-blade mistuning. The remaining variance between the experimental and analytical results may be either due to noise in the TSD, numerical mistuning due to element warping cause by MORPH, material variation within the IBR, and/or experimental error.

Despite the small standard deviation within the repeated experimental results ($\sigma < 0.03\%$), the blade-blade mistuning amplification prediction from FMM ID exhibited significant variation in blade response amplification from the tuned system. Figure 6, the mistuned amplification for experimental data can range nearly an order of magnitude for a given blade due repeated experimental runs. The variation is far greater for low energy blades whose maximum amplification is less than or equal the tuned response, while for the high responding blades, blades 16 and 17 for this rotor, the relative variation in maximum response is far less. This demonstrates the sensitive and often chaotic nature of mistuning prediction. However, despite the large variation, the GMM analysis correctly predicts the response of the two highest responding blades in the IBR. This is laudable considering the complexities of optically measuring an IBR, converting that data into a FEM, and recognizing that the finite elements are approximations of the physics that have degraded capabilities caused by warped elements induced through complex geometry.

An additional source of variation between the experimentally based FMM ID predicted amplification and the analytical based amplification is the accuracy of mode shape extraction. The system mode shapes for a given blade mode are orthogonal by definition; the 22 system modes are distinct and decoupled. However, when a system mode is not exhibited strongly in a single blade the signal to noise ratio falls significantly such that orthogonality of a given mode shape is called into question. Given that low energy blades will also have lower signal to noise ratios even for highly excited system modes, the blade amplification prediction of those same blades are poorly represented through FMM ID. This is demonstrated in Figure 7 where there is strong agreement between all three methods of blade response prediction for the high responding blades, and poor agreement for the low responding blades. For the analytical results, while the mode shapes can be extracted from a FEM accurate to double precision floating point the numerical inaccuracy of the FEM,

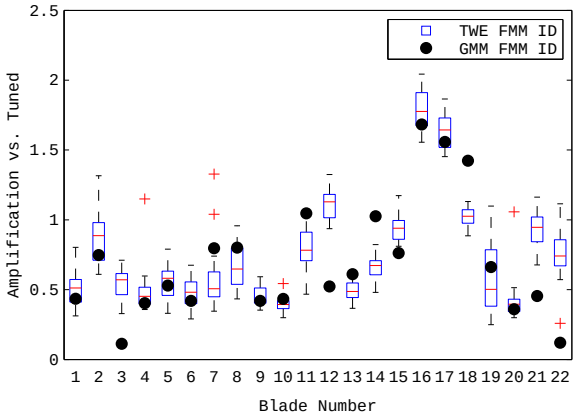

Figure 6: Variation in Blade Amplification from FMM ID Analysis

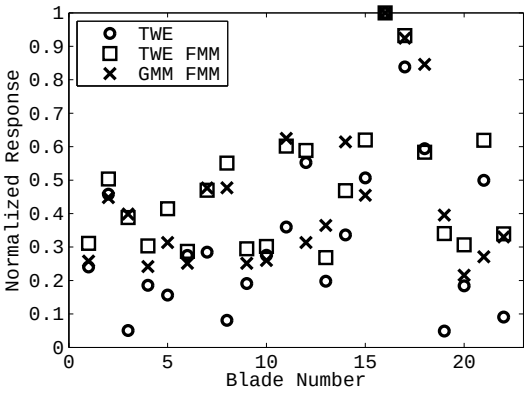

Figure 7: Experimental to FMM ID Amplification

both in surface node position and element shape, contribute to a potentially inaccurate model. While this model accurately predicts the relative amplitude magnification of the high responding blades, the false high responder blade 18 is likely due to the overestimation of sector mistuning according to 5.

The reader may question why FMM ID is even necessary if the mistuned amplification can be inferred directly (and possibly more accurately) from the experimental data according to Figure 7. While the blade to blade response variation from experimentally obtained data can be analyzed to determine relative blade response, the relative amplification from an ideal tuned IBR is in-determinant; the experimental model cannot directly predict the tuned response, it must be estimated using an alternative method (e.g. FMM ID). Figure 7 shows relative blade amplifications, and while useful for blade to blade relative amplification comparison, it does not show the tuned to mistuned amplification and can only assume a normalized response from the experimental results. In fact, this is a step in the calibration method: all blades are normalized to the highest responding blades. In the repeated analysis the amplitude of blade 16's FRF is invariant while the remaining blades show an average variation of 0.2 in their normalized response relative to the high responding blade. This indicates as much as a 20% error in mode shapes computed downstream from this data, and while the least squares optimization approach to solving for tuned system frequencies and sector mistuning places higher weighting on more orthogonal mode shapes, blade response variations in Figure 6 clearly indicate that mode shape accuracy imparts significant error to blade amplification prediction.

B. Repeated High Fidelity Optical Scan

Given the highly sensitive nature of mistuning and the noise inherent within the optical scan data, five scans were taken of the production IBR with a programmable mechanical scanner. This programmable scanner allows for an identical number of image captures per blade and eliminates variation in capture location caused by manual scanning. Additionally, the programmable mechanial arm allowed for a smaller scanning volume (6.7 in $\times$ 6.7 in $\times$ 6.7 in) resulting in lower noise and denser point cloud. The five TSD models contained approximately $4 \times 10^6 \pm 2 \times 10^5$ geometric points. While each point cloud was collected using a carefully controlled, closed loop process, the origin of each point cloud shifted by a significant margin and each cloud had to be realigned individually to the nominal CAD. Therefore, the variation between models, shown in Figure 8 shows not only the noise between the optical scans, but the alignment error as well. This figure is shown with a narrow scale where green represents intra-scan error less than 0.0002 in and red represents greater 0.0005 in. The ICP alignment algorithm does not appear to contribute to intra-scan error given the near identical noise pattern on each blade. The mean scan to scan variation is 0.00017 in and the areas of highest noise were the blade tips, leading and trailing edges, and platform/disk. The roughened surface of the IBR, due to shot peening, allowed for more light scattering and reduced collection noise, while the disk, only slightly shown in the core of Figure 8, was the noisiest portion of the IBR. The optical scanner was found to be less accurate in the "shadow" areas on the trailing edge near the disk of the IBR where it was difficult for both camera heads on the optical scanner to maintain line of sight on the surface of the IRB. This is a critical portion of the IBR to have poor accuracy given the importance of an accurate blade to disk interface.

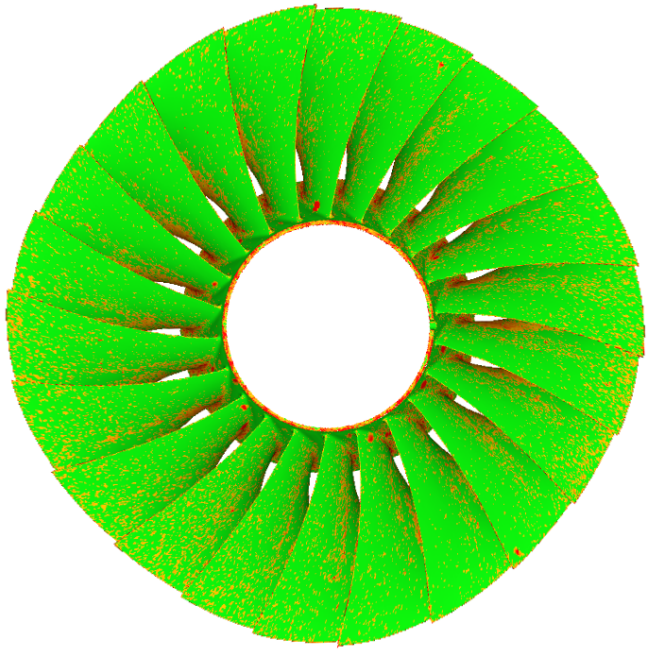

Figure 8: Multiscan Variation (Geometrically Skewed)

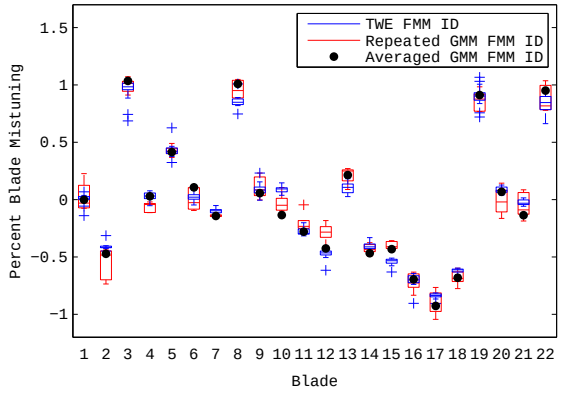

Figure 9: Mistuned Sector Variation with Repeated Scans

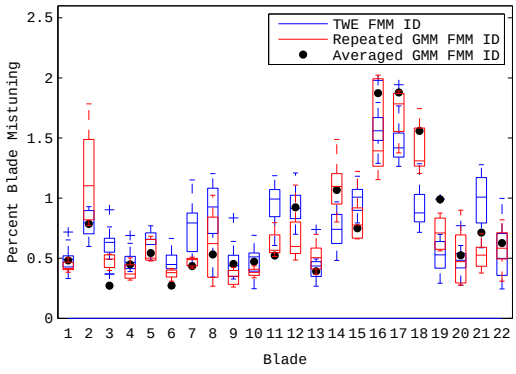

Figure 10: Blade Amplification with Repeated Scans

Using the same nominal FEM, five new GMMs were generated individually from the repeated scan data and an additional GMM was generated by averaging all five repeated scans to attempt noise reduction. Figure 9 shows the variation in the sector mistuned frequencies calculated using FMM ID for 1T and compares this to the variation in the repeated experimental data. The variation in the repeated scans is greater than

that obtained by the experimental data, and as shown in Figure 10, this significantly affects blade response amplification. For example, the large variation in blade alone frequency of blade 2 causes it to become a tuned absorber in the case where its sector mistuning deviation falls below 0.6%, causing the response amplification to rise far above the experimental results. Averaging the results results in a much higher correlation with the experimental data in both sector mistuning (R^2 of 0.9729 vs. 0.9484) and the GMM obtained from the averaged scan data accurately identifies the two highest responding blades.

The large variability in both the sector mistuning and relative blade amplification underscores the complexity of the geometry to FMM ID results process. Noise from the TSD propagates into the mesh metamorphosis process and varies the converged locations of the FEM surface nodes due to variations in the neural network. These surface node variations propagate inward and potentially cause numeric mistuning, and the results of the modal analysis are then interpreted using FMM ID, already shown to be an approximate approach in representing relative blade amplifications. Accounting for the sensitivity and chaotic nature of mistuning amplification, the variation in blade amplification, even with repeated point clouds with a mean variation of 0.00017 in, is reasonable and demonstrates the need for high fidelity GMMs to accurately capture mistuning amplification.

C. Multi-variable Convergence Study

Thus far, the density of the point cloud and the FEM have been constant for all GMMs with a relatively coarse FEM containing approximately 200,000 nodes. As mistuning has been shown to be highly sensitive for even the smallest variations in geometry from the repeated scans, blade amplification is likely highly sensitive to variations in FEM and TSD density. This section investigates the effect of model and geometry density on model accuracy by correlating the GMM FMM ID results to the TWE FMM ID results as in the prior two sections.

The original TSD was decimated into 9 separate point clouds ranging in size from 250,000 points to the original 4 million points. The point density of the model was intelligently varied to optimize accuracy along high curvature areas (e.g. blade tips) in order to simulate actual optical scans as modern optical scanning software concentrate geometry points. Six FEMs were generated from the same original CAD containing a structured hexahedral mesh for the blade and platform region, a narrow tetrahedral and pyramidal interface within the disk, and an unstructured hexahedral mesh within the central disk. Mesh density was varied by modifying the average edge length, meshing a single sector, and cyclically replicating the sector to generate full models ranging from approximately 80,000 nodes to 800,000 nodes. Each nominal model was MORPHed to each TSD and 54 mistuned models were generated, solved, and post processed using FMM ID to compute sector mistuning and blade amplification.

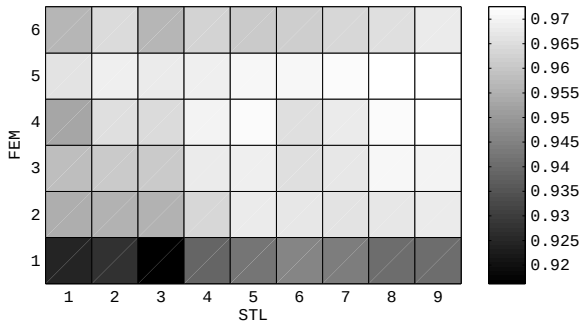

Figure 11: Sector Mistuning Correlation

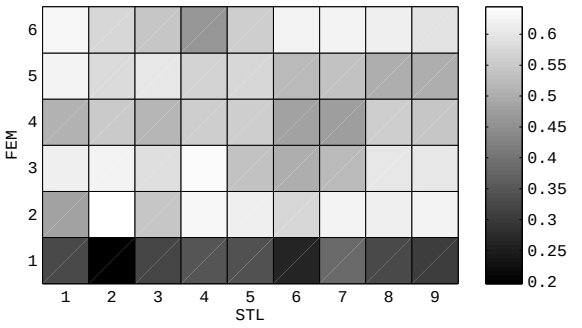

Figure 12: Blade Amplification Correlation

The results from the convergence study show a strong positive correlation to both TSD and FEM density for sector mistuning. Figure 11 shows that the sector mistuning begins strongly with a R^2 of 0.92 for the coarse FEM and TSD and increases to 0.97 for the denser models. The density of the optical scan data has a stronger effect on the correlation than the FEM density further reinforcing the conclusion in the repeated scan section that geometric accuracy is tantamount for GMM accuracy.

There appears to be a weak correlation for all but the coarsest FEM to blade amplification accuracy according to Figure 12. However, the correlation results are based on all 22 blades and given the large variation even among the experimental data for low responding blades, these results do not accurately capture the convergence that is actually occurring. As the goal of the GMM digital twin model is to detect and predict maximal amplification, results for blades 2 and 16 can be used to show how the false positive and maximum responding blade converge. The false positive blade 2 which occurred in a portion of the repeated scans shows a high sensitivity to mesh density and TSD density. The large blade amplification variation is due to the sector mistuning patter (high low high), and the blade is on the boundary of becoming a tuned absorber for the system (as blades 16 and 17 are). Due to this, even the smallest variation in the FEM for this sector causes modal energy confinement leading to blade amplification. Figure 13 shows the blade amplification results for blade 2 for all six FEMs across all 9 STLs with the thicker lines belonging to the denser FEMs. GMM convergence is clearer given this example as the converged amplification, 0.8 of the tuned response, is within the TWE result range. This occurs likewise for the high responding blade 16, and Figure 14 shows the GMMs converging to an amplification of 1.75, also in strong agreement with the TWE results.

Therefore, while the blade amplification correlation is low for the remaining blades, the response of those blades is irrelevant as they respond with less energy than their tuned counterparts. The sector frequency deviation, however, is critical for the accurate computation of the high responding blades, and the GMM clearly succeeds in that respect given $R^2 > 0.97$ for the high density FEM and TSD. The key takeaway from this section is the GMM is sensitive to FEM and TSD density, especially in regards to blades on the cusp of becoming tuned absorbers. As the highest density TSD and FEM took only 20 minutes to generate, MORPH, analyze, and post process on a quad core 3.5 GHz Intel Xeon platform, the digital twin approach is clearly within the limits of modern computing power.

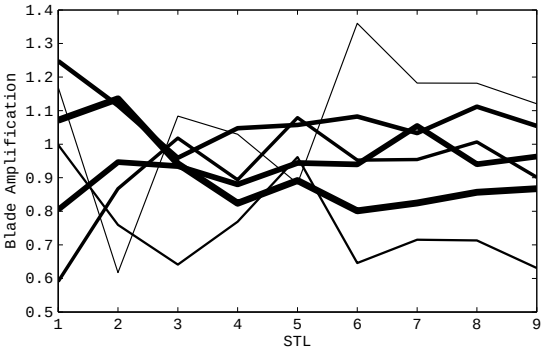

Figure 13: Blade 2 Amplification Convergence

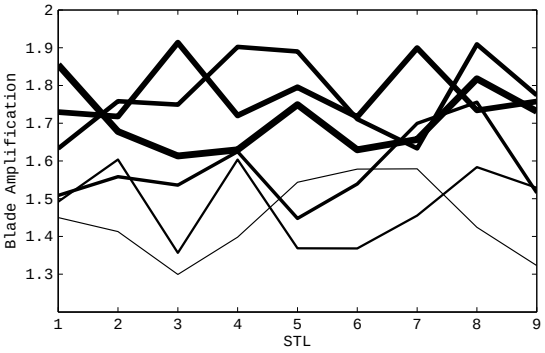

Figure 14: Blade 16 Amplification Convergence

D. Material Variation

This research has established that a GMM accounts for blade mistuning variation accurate to an R^2 equal to 0.9729. Having minimized the noise inherent within TSD obtained from an optical scanner as well as numerical inaccuracy due to FEM density, the remaining sources of error include experimental error, FMM ID approximation error, and variation in material properties. Setting aside experimental error and FMM ID error, the effect of material property error can be established with two analyses. First, varying the global modulus to determine its effect on the mode shapes and therefore FMM ID accuracy, and second, modifying sector elastic modulus to match the average TWE sector mistuning results. Results from the first analysis will show if it is necessary to have accurate estimates of an IBR's material properties, or if a nominal properties can be used. The second analysis will determine how much of the remaining variation arises purely from inaccuracies in sector frequency mistuning, which, assuming that the geometry has been fully captured in the analytical, is driven by variations in elastic modulus.

The global elastic modulus of the analytical model was varied from -4 % of the nominal value used in the prior analyses to + 4% in 0.04% steps. A ±4% variation in Global elastic modulus variance caused virtually no difference in the blade amplification resulting from FMM ID or its correlation to experimental data (within ± 0.005). Mathematically speaking, changing the elastic modulus merely scales the system

frequencies ω_j without varying the sector frequency deviations β_j resulting from Equation **??**. As scaling elastic modulus within the analytical model will vary the eigenvalues, but not the eigenvectors of the solution to the FEM eigenproblem, the mode shapes will remain constant. Therefore, global modulus accuracy not necessary for accurate FMM ID prediction since blade amplifications within FMM ID are dependent on relative sector mistuning and relative tuned system frequencies.

To account for potential material variations, the discrepancy between the TWE FMM ID mistuning and GMM FMM ID mistuning was adjusted by modifying the individual material properties of each blade.

III. Conclusion

Mistuned response is highly chaotic and shows significant variation even given experimental data collected from a carefully controlled and repeated experiment. The strong agreement in maximal blade amplification prediction as exhibited by this research is a significant accomplishment and indicates that optically based GMM analysis is a potential tool for mistuned response prediction. This GMM process can be applied in several manners. Accurate geometry collected from a variety of sources can be used to generate the GMM for a single rotor for an accurate response prediction rotor over several modes. For a population analysis, the geometry of a large population can be estimated by boot-strapping from a subset of that fleet's geometry data using principle component analysis in order conduct a deterministic fatigue analysis. This approach will likely yield far more realistic results than a Monte Carlo simulation as the models will be based on actual, rather than random, geometry perturbations. Additionally, this mistuning response prediction approach may avoid the complexity of utilizing reduced order models in FEA due as a deterministic analysis would require a smaller number of FEA analyses and given that an accurate model was obtained with only 250,000 nodes, requiring only a modest amount of memory and computation time even for a modern desktop computer.

Further research includes extending this GMM based mistuned response prediction to other rotors with potentially varied material properties to determine the basis for relying solely on the GMM, experimentally obtained results, or both. Such a study would reveal when material variations within a population are statistically irrelevant or when they should be included as a factor of uncertainty. As the repeated experimental analysis indicated a large variation in the experimental results as well as the results obtained from FMM ID, further research should be conducted in validating the both the calibration approach and repeatability of the TWE experiment. Additionally, given the likely presence of noise in the TSD, a critical analysis of the optical scan data through repeated data collections of a single IBR using multiple scan volumes (enabling varied accuracy and point cloud density) will help to bound the potential for error in the mistuned blade response prediction from the GMM.

Research in this paper shows that a full 360° digital twin model of the IBR to be sufficient in predicting mistuned response and has been validated by experimental results. As measured GMM based analysis has the potential to significantly extend fleet IBR lifetimes as an aircraft maintainer will have more accurate knowledge of the geometry and mistuned response of the rotor given wear and damage caused by ordinary operations. Not only can this allow for rapid engine response prediction without the utilization of strain gauge or non-intrusive stress measurement systems (NSMS), but could also lead to the incorporation of optical scanning and subsequent response prediction in operation and sustainment for United States Air Force.

References

[1]Brajlih, T., Tasic, T., Drstvensek, I., Valentan, B., Hadzistevic, M., Pogacar, V., Balic, J., and Acko, B., "Possibilities of Using Three-Dimensional Optical Scanning in Complex Geometrical Inspection," *Strojniki vestnik - Journal of Mechanical Engineering*, Vol. 57, No. 11, 2011.

[2]Glaessgen, E. and Stargel, D., "The Digital Twin Paradigm for Future NASA and U.S. Air Force Vehicles," *53rd AIAA/ASME/ASCE/AHS/ASC Structures, Structural Dynamics and Materials Conference*, 2012.

[3]Tuegel, E., Ingraffea, A., Eason, T., and Spottswood, S., "Reengineering Aircraft Structural Life Prediction Using a Digital Twin," *International Journal of Aerospace Engineering*, Vol. 2011, No. 14, 2011.

[4]Tuegel, E., "The Airframe Digital Twin: Some Challenges to Realization," *53rd AIAA/ASME/ASCE/AHS/ASC Structures, Structural Dynamics and Materials Conference*, 2012.

[5]"High dynamic range fringe acquisition: A novel 3-D scanning technique for high-reflective surfaces," *Optics and Lasers in Engineering*, Vol. 50, No. 10, 2012, pp. 1484 – 1493.

[6]Castanier, M. and Pierre, C., "Modeling and Analysis of Mistuned Bladed Disk Vibration: Current Status and Emergin Directions," *Journal of Propulsion and Power*, Vol. 22, No. 2, 2006.

[7]Fleeter, Y. C. D. G. S., "Analysis of Structural Mistuning Effects on Bladed Disc Vibrations Including Aerodynamic Damping," *International Compressor Engineering Conference*, 2004.

[8]Castanier, M. and Pierre, "Dynamic Response Predictions for a Mistuned Industrial Turbomachinery Rotor Using Reduced-Order Modeling," *Journal of Engineering for Gas Turbines and Power*, Vol. 124, No. 2, 2002, pp. 311–324.

[9]Beck, J., Brown, J., Slater, J., and Cross, C., "Probabilistic Mistuning Assessment Using Nominal and Geometry Based Mistuning Methods," *Journal of Turbomachinery*, Vol. 135, No. 5, 2013.

[10]Remondino, F. and El-Hakim, S., "Image-based 3D Modelling: A Review," *The Photogrammetric Record*, Vol. 21, 2006, pp. 269–291.

[11]Pauly, M., Mitra, N. J., and Guibas, L. J., "Latest Optical Methods for Industrial Dimensional Metrology," *Eurographics Symposium on Point-Based Graphics*, Zurich, SWI, 2004.

[12]Kaszynski, A., Beck, J., and Brown, J., "Uncertainties of an Automated Optical 3D Geometry Measurement, Modeling, and Analysis Process for Mistuned Integrally Bladed Rotor Reverse Engineering," *Journal of Engineering for Gas Turbines and Power*, Vol. 135, 2013.

[13]Benzley, S. E., Perry, E., Merkley, K., and Clark, B., "A Comparison of All Hexagonal and All Tetrahedral Finite Element Meshes for Elastic and Elasto-plastic Analysis," *4th International Meshing Round table Sandia National Labs*, Provo Utah, 1995.

[14]Kaszynski, A., Beck, J., and Brown, J., "Automated Finite Element Model Mesh Updating Scheme Applicable to Mistuning Analysis," *ASME Turbo Expo*, 2014.

[15]Moller, T. and Trumbore, B., "Fast, Minimum Storage Ray-Triangle Intersection," *Journal of Graphics Tools*, Vol. 2, 1997, pp. 21–28.

[16]Bottasso, C., Detomi, D., and Serra, R., "The Ball-Vertex Method: A New Simple Spring Analogy Method for Unstructured Dynamic Meshes," *Computer Methods in Applied Mechanics and Engineering*, Vol. 194, 2005, pp. 4244–4264.

[17]Vartziotis, D. and Wipper, J., "Fast Smoothing of Mixed Volume Meshes based on the Effective Geometric Element Transformation Method," *Computer Methods for Applied Mechanical Engineering*, Vol. 201-204, 2012, pp. 65–81.

[18]Holland, D., Castanier, M., Ceccio, S., Epureanu, B., and Filippi, S., "Testing and Calibration Procedures for Mistuning Identification and Traveling Wave Excitation of Blisks," *Journal of Engineering for Gas Turbines and Power*, Vol. 132, No. 4, 2010, pp. 9.

[19]Feiner, D. and Griffin, J., "Mistuning Identification of Bladed Disks Using a Fundamental Mistuning ModelPart I: Theory," *Journal of Turbomachinery*, Vol. 126, No. 1, March 2004, pp. 150–158.

[20]Feiner, D. and Griffin, J., "Mistuning Identification of Bladed Disks Using a Fundamental Mistuning ModelPart II: Application," *Journal of Turbomachinery*, Vol. 126, No. 1, March 2004, pp. 159–165.